Structural and thermal characterization of zirconia/hydroxyapatite composites prepared via sol-gel for biomedical applications

M. Catauro[*, 1], F. Bollino[1], E. Tranquillo[1], R. Tuffi [2], A. Dell'Era [3], S. Vecchio Ciprioti [*, 3]

[1] *Department of Industrial and Information Engineering, University of Campania "Luigi Vanvitelli", Via Roma 29, I-81031 Aversa, Italy*

[2] *Department of Sustainability, ENEA – Casaccia Research Center, Via Anguillarese 301, Rome, Italy*

[3] *Department of Basic and Applied Science for Engineering, Sapienza University of Rome, Via Del Castro Laurenziano 7, I-00161 Rome, Italy*

*Corresponding authors: michelina.catauro@unicampania.it
Phone: 0039 0815010360
Fax: 0039 0815010204
(Michelina Catauro)

stefano.vecchio@uniroma1.it
Phone: 0039 0649766906
Fax: 0039 0649766947
(Stefano Vecchio Ciprioti)

Abstract

The thermal behavior of pure ZrO_2 and hydroxyapatite (denoted as Z and HAp, respectively), as well as three composites with different content of Z and HAp (Z90HAp10, Z70HAp30 and Z50HAp50) prepared via sol-gel method has been studied by thermogravimetry (TG) and first-order derivative of TG up to 1200°C under inert gas atmosphere. Dehydration, loss of alcohol and acetylacetone and a multi-step thermal decomposition processes has been identified by analyzing the gases evolved in each step by Fourier transform infrared spectroscopy (FTIR). Fresh samples of Z-rich composites undergo an abrupt ejection of material from the crucible around 200°C with noticeable increase of the sample temperature. During the occurrence of this phenomenon FTIR spectra demonstrated the evolution of gases (CO, CO_2, acetone and ethylene) due to the simultaneous decomposition of acetylacetone and ethanol, not present in the samples calcined at 120°C. As far as the structural study is concerned, pure Z crystallizes at 1000°C in the monoclinic system, but the presence of HAp in the composite materials enables the crystallization of Z in the

tetragonal phase. Finally, the amorphization degree increases with increasing the content of Z in all the composites treated at 600 and 1000°C.

Keywords: sol-gel process; hydroxyapatite; crystallization of zirconia; TG-FTIR analysis

1. Introduction

Glass and ceramics with several compositions are materials widely proposed for biomedical applications, mainly in dental and orthopedic fields. Bioactive glasses, indeed, exhibit ability of forming biominerals on their surface, which attracts bone building osteoblast cells. From the development of the first bioglass by Hench at al. (denoted as 45S5), many compositions of bioglasses were explored in order to obtain biomaterials with enhanced performance. Among these, zirconia (ZrO_2) and zirconia-based glasses and ceramics, as well as calcium phosphates, with particular reference to hydroxyapatite (HAp), have attracted considerable interest in the recent years [1-10]. Their use, indeed, have several advantages. Studies proved that when zirconia-based prosthesis were implanted in vivo, they are encapsulated by connective tissue and, thus, no local or systemic toxic effects were recorded neither in soft nor in hard tissues after their implantation [3, 5]. Moreover, no release of residues or degradation phenomena were detected and a low bacterial growth was recorded [3, 5].

Both crystalline and amorphous zirconia and zirconia-based materials have shown interesting biological performances. Amorphous zirconia-based glasses were proposed as matrices for drug delivery [2, 11], or as bioactive coatings [12-15], showing the ability to improve cell viability of human osteosarcoma cell line [13] and human mesenchymal stromal cells [15]. Yttrium-stabilized tetragonal zirconia or tetragonal zirconia polycrystal (TZP) was used in orthopaedics (as hip head prostheses) [16], and in dentistry for root canal posts, fixed partial dentures and dental implants [17]. On the other hand, as far as the biomedical applications are concerned the interest in calcium phosphate-based ceramics [4, 18-23] for bone repair and substitution stems from their bioactivity (i.e. the capability to bond with the living bone by the formation of an hydroxyapatite layer on their surface with a composition similar to that of the mineral phase of bone [24]). In particular, the interest for crystalline HAp and HAp-based ceramics as materials for artificial bones and scaffolds for tissue engineering [25], is due to their similarity with biological apatites present in bones and teeth that leads to high affinity with host tissue and, thus, to an excellent bioactivity and

biocompatibility. However, their poor mechanical properties that limit their usage in several clinical application, induced researchers to develop composites consisting of synthetic hydroxyapatite and TZP fillers to reinforce the HAp structure [26-29]. Moreover, composites mainly consisting of zirconia containing different amount of synthetic HAp were recently proposed [30], where addition of HAp led to an improvement of the biological performance of pure zirconia. The ZrO_2/HAp composites were obtained by mean of the sol-gel method, a process used to manufacture glass and ceramic oxides at low temperature. The synthesis procedure involves the hydrolysis of a metal alkoxide precursor dissolved in a water-alcohol solution and the condensation of the formed oligomers. Those reactions cause the transition from the starting colloidal solution named "sol" into a 3D network, namely "gel". A heat treatment of the gel is required to allow the removal of the residual solvents and the densification of the materials. Modifying the gel heating conditions results in modulating the structure and, thus, the properties of the obtained materials. The temperature and heating rate of the heating treatment, indeed, are well known key factors in determining the final microstructure of glass and ceramic sol-gel materials. For example, a xerogel can be obtained using low temperatures, whereas solvent extraction under supercritical conditions is requested to produce an aerogels. Moreover, different heating conditions can lead to amorphous or crystalline materials. As a different degree of crystallization leads to a variation of the ion release from the materials, it can influence also material biological performances as observed for ZrO_2/HAp composites and other sol-gel bioglasses [30, 31]. The dissolution rate of a bioactive glass, indeed, plays a key role in its usage as implant because can cause alterations in the mechanical properties of the material as well as variation in its surface charge, thus leading to a modification in the protein adsorption and hydroxyapatite nucleation ability.

Therefore, the in-depth knowledge of thermal decomposition of the dried gels is essential and the determination of the optimum condition for the calcination of the sol-gel materials is required to obtain the desired biomaterial [32-38]. The present study inserts in this context and has the aim of investigating into the thermal degradation phenomena and the structural modifications that take

place when the previously synthesized sol-gel ZrO_2/HAp composites [30] were submitted to heating. To this end, the thermal behavior and the mechanisms of the thermally stimulated processes were studied by evolution gas analysis (EGA), similarly to what has been carried out in the past [39]. In this study, the EGA system has been realized by coupling a thermal analysis equipment with a Fourier transform infrared spectroscopy (FTIR) unit. This information is necessary to explain the relation between the different biological responses recorded after exposure to the materials and the temperatures of the applied post-synthesis heat treatments, and to identify the better conditions to be used for obtaining bioimplants with relevant biological performances.

2. Materials and methods

Sol–gel synthesis

Composites with chemical formula $xZrO_2(1\text{-}x)HAp$ (where x = 1, 0.9, 0.7, 0.5, 0 indicates the mole fraction of ZrO_2 in the composites) were synthesized by means of the sol-gel method as reported elsewhere [30]. The pure ZrO_2 was obtained using a zirconium propoxide solution (70 wt. % in 1-propanol, Sigma-Aldrich, Milan, Italy) as metal alkoxide precursor. The precursor was added to a solution of acetylacetone (AcAc, Sigma-Aldrich, Milan, Italy), a chelating agent used to inhibit the fast hydrolytic activity of zirconium propoxide, in pure ethanol (99.8% Sigma-Aldrich, Milan, Italy). The molar ratios between the reagents achieved in the obtained sol are the follows: $Zr(OCH_2CH_2CH_3)_4$ /AcAc = 3 and EtOH/$Zr(OCH_2CH_2CH_3)_4$ = 6.

To synthesize pure HAp, calcium nitrate tetrahydrate ($Ca(NO_3)_2 \cdot 4H_2O$, Sigma-Aldrich, Milan, Italy) and phosphorus pentoxide (P_2O_5, Sigma-Aldrich, Milan, Italy) were used as precursor, where $Ca(NO_3)_2 \cdot 4H_2O$ was dissolved in pure ethanol under magnetic stirring. The resulting solution was then added under stirring to a previously prepared solution of P_2O_5 in NH_4OH and pure ethanol at pH=11, thus obtaining a molar ratio Ca/P in the final solution equal to 1.67.

The composites samples were synthesized by adding drop by drop and under stirring adequate amounts of zirconia sol to the HAp one, until a homogeneous and transparent solution was

obtained. Then, the composites sols were left to gel at room temperature and the obtained wet gels dried at 40°C for 2 hours.

Thermal and evolution gas analyses

The thermal behavior of the pure ZrO_2, HAp and composites was studied by means of a simultaneous Mettler Toledo TG/DSC 2950 instrument, being the experimental raw data processed by a STARe software. The instrument has been equipped with two identical crucibles, one for the reference filled with alumina in powder form and one for the sample, containing about 20–25 mg of solid in order to uniformly cover the bottom surface area of the crucible. The TG experiments were carried out under an inert nitrogen flowing atmosphere (60 mL min^{-1}) up to 1200 °C at a heating rate of 10°C min^{-1}. The sample temperature was calibrated by performing identical experiments using very pure indium and zinc reference materials (purity higher than 99.998%), and assuming a final average uncertainty $u(T)$=±1K over the whole temperature range explored.

The mechanisms of thermally activated processes during the occurrence of TG/DSC experiments were identified using a SETARAM 92-16.18 TG apparatus coupled by a Thermofisher Scientific Nicolet iS10 Spectrophotometer. The apparatus has been equipped with 250 μL alumina crucibles, filled with about 100-150 mg of sample to obtain the minimum amount of gaseous species to be analyzed by FTIR using the Calisto software. A preliminary blank experiment was performed using empty crucibles under the same experimental conditions of the samples tested (argon purging gas at 40 mL min^{-1}, in the temperature range between 25 and 1200°C at a constant heating rate of 10°C min^{-1}). The vapors evolved during the TG experiments were conveyed to the FTIR apparatus through a heated transfer line kept at 200°C. The instrument is able to collect a spectrum each 11 s, being eight scans performed at 0.5 cm^{-1} intervals with a resolution of 4 cm^{-1}.

XRD analysis

After the thermal treatment of the samples powders for 2 h under a argon purge gas atmosphere at 120, 600 and 1000°C (temperatures selected on the basis of a careful examination of their thermal behavior shown by the TG curves), the crystalline phases have been identified by X-ray diffraction (XRD) analysis by means of a Philips diffractometer, equipped with a PW 1830 generator, where the source of X-ray is given by a Cu-Kα radiation with λ=0.15418 nm.

Results and Discussion

Thermal behavior study

The TG/DTG curves of fresh samples (not thermally treated) of pure zirconia and HAp (Z and HAp, respectively) and of composites containing different amount of both components (Z90HAp10, Z70HAp30, Z50HAp50) are shown in Fig. 1. In particular, the thermal behavior of pure Z and HAp and Z50HAp50 in Fig. 1a seems to be, as expected. The TG/DTG curves of pure Z, recently examined elsewhere [36], show a first mass loss up to about 150°C, probably due to dehydration. By analyzing the gases evolved during the TG experiment a more complex degradation occurs.

The second step of mass loss between 150 and 230°C is mainly due to dehydroxylation that leads to the release of water by condensation of the surface hydroxyl groups. Fig. 1a shows a third step of mass loss between 300 and 470°C, followed by a final step (with about 5% of mass loss) in the range 480-600°C.

Pure HAp undergoes a first two-stage process up to about 200°C, accompanied by a mass loss of more than 30%, ascribed to the release of water differently bound to the material. After this process, some slow parallel and consecutive mass losses took place up to 580°C, the first of which seems to proceed through a two-stage pathway between 200 and 380°C, followed by two more distinguishable steps in the temperature ranges 380-490°C and 490-580°C, respectively. The composite material containing equimolar amount of Z and HAp (Z50HAp50) shows a thermal

behavior representing a sort of average of those of the pure components, but with more defined and evident effects (DTG peaks are sharper than those of Z and HAp). The total amount of water adsorbed up to 200°C (with three distinct DTG peaks) does not exceed 20%, while the dehydroxylation and degradation steps seem to occur at temperatures higher than those of pure HAp and end at 600°C. On the other hand, the two poor-HAp composites (with 0.1 and 0.3 molar fractions of HAp, denoted as Z90HAp10 and Z70HAp30, respectively) undergo an explosive thermal behavior around 200°C that caused the ejection of significant amount of both the samples from the crucible during their TG experiments, as it can be seen in Fig. 1b. This phenomenon occurred in Z90HAp10 and Z70HAp30 is accompanied by evolution of heat that caused an anomalous increase of the sample temperature with time in comparison with the expected programmed linear one (Figs. 2a-f, particularly evident in Figs. 2c and 2f the black circles).

The TG/DTG curves of all the samples (after a thermal treatment at 120°C) are shown in Fig. 3, where a careful examination of their shapes seems to suggest that the thermal treatment at relatively low temperature does not modify significantly the thermal behavior of these composites, except for the absence of the abrupt mass loss occurring in the Z90HAp10 and Z70HAp30, accompanied by evolution of heat and ejection of mass from the crucible. In general, the thermal treatment at 120°C seems to stabilize the two composites (in spite of the relatively low temperature), and the water evolved is partly adsorbed (from water vapor on cooling), and subsequently lost in these TG new experiments at lower temperature (even though because it is probably physically bound to the materials).

FTIR-EGA analysis to identify the mechanisms of thermally stimulated processes

Fig. 4 shows the FTIR spectra of the gas mixture evolved during the TG experiments of Z, HAp, and of their composites at different temperatures. In particular, the FTIR spectrum of the gases released from sample Z at 115°C (corresponding to the first step of mass loss in Fig. 1a) revealed an initial evolution of propanol, water and acetone. Propanol is produced by hydrolysis and

196 condensation reactions, which involve zirconium propoxide as precursor, and its release is proved
197 by the intense bands at 2970 cm^{-1} and the doublet at 1065 cm^{-1}, with a shoulder at 980 cm^{-1}
198 ascribable to the stretching of C-H and C-C bonds, respectively, along with the signals in the region
199 1200-1500 cm^{-1} ascribable to the C-H bending modes. The stretching of the hydroxyl functional
200 group, generally visible at 3670 cm^{-1}, is covered by the signals of water. At this temperature,
201 indeed, the adsorbed water is also released as proved by the several sharp bands in the ranges 4000-
202 3400 cm^{-1} and 1850-1280 cm^{-1}. In the latter range a strong signal at 1745 cm^{-1} (due to the stretching
203 of C=O bond) is also visible that, together with the peaks at 1220 cm^{-1} and 1365 cm^{-1} (due to C-H
204 and C-C deformations, respectively), proved the formation of acetone. That is the main product of
205 the thermal degradation of the acetylacetone bonded to zirconium (acetylacetonate of zirconium)
206 together with carbon dioxide [40]. Typical signals of CO_2, indeed, also are visible as a doublet at
207 2355 cm^{-1}, 2320 cm^{-1} and a sharp peak at 670 cm^{-1}. The water signals are still visible in the FTIR
208 spectrum of the gas evolved at 187°C. Moreover, propanol residue is found, whereas the increase of
209 the intensities of the acetone and CO_2 signals suggests that the thermal degradation of acetylacetone
210 continues even at higher temperature. The FTIR spectrum of Z at 378°C reveals in Fig. 4 the
211 intensities of characteristic bands of acetone decreasing, until these signals almost disappear in the
212 spectrum at 523°C. However, at the same time the intensity of bands related to CO_2 increases and
213 the appearance of sharp peaks at 1300 and 3015 cm^{-1} in the spectrum at 523°C suggests that the
214 acetone formed, in turn, degrades leading to the release of methane and CO_2 [40, 41]. Both the
215 mechanisms of the thermal events occurring around 378°C and 523°C are easily identified. The
216 former is related to the initial formation of nucleus of tetragonal zirconia (*t*-ZrO_2) after
217 dehydroxylation that via condensation of the –OH residue groups located on the materials surface,
218 while the second to the bulk crystallization, in agreement with the literature findings [42]. This
219 hypothesis is also confirmed by the presence of water signals in the FTIR spectra of the gas evolved
220 recorded at 523°C.

The FTIR spectrum of the gas evolved during the TG experiment of pure HAp sample at 122°C reveals the presence of water, CO and CO_2. Water released can be due to the removal of the adsorbed, hydration water [43, 44], or by crystallization water contained in calcium nitrate [45], as well as by water produced by the partial combustion of the ethanol [26]. The presence of the signal typical of CO and CO_2 (the doublets at 2355 - 2320 cm^{-1} and 2230 - 2200 cm^{-1} respectively), indeed, suggests that an incomplete combustion of organic matter occurs in this material, which could be caused by oxygen released from the materials pore. The spectrum of HAp at 171°C shows, in addition to water, CO and CO_2, the presence of some signals ascribable to other gas species. They appear very noisy because overlapped with the water signals. In particular, the weak bands in the range 3000-2800 cm^{-1} and those at 1040 cm^{-1} and 1170 cm^{-1}, indicate that an initial release of ethanol occurs around this temperature. Moreover, the presence of the doublet at 1589 – 1623 cm^{-1}, suggests that also the release of nitrogen oxide or nitric acid takes place. The thermal degradation of nitrate salts, generally proceeds through dehydration followed by the emission of N_2O_5 (or of a gas mixture composed by NO_2 and O_2 in a molar ratio 4:1) [45]. However, in some cases an initial release of nitric acid was recorded [46]. Therefore, the presence of noise makes difficult to distinguish between nitrogen oxide or nitric acid, whereas the temperature suggests that the signals are due to the development of nitric acid. The intensities of signals attributed to ethanol increase in the FTIR spectrum recorded at 223°C (Fig. 4), and the strong band at 1740 cm^{-1} can be ascribed to the stretching of C=O of acetaldehyde. Pyrolysis of ethanol can proceed through two alternative mechanisms: dehydration with formation of ethylene and water, or dehydrogenation leading to the formation of acetaldehyde and hydrogen (undetectable by FTIR) [47]. The presence of the bands at 2800 cm^{-1} and 2700 cm^{-1}, typical of the C-H vibrations in the aldehyde groups [48], confirms the presence of acetaldehyde. In the spectrum recorded at 263°C the signal of ethanol, CO, CO_2 and acetaldehyde are still evident. In addition, the weak sharp band at 948 cm^{-1} can be due to the formation of ethylene. The intensity of this signal (as well as that of CO_2) increases in the spectrum recorded at 309°C, whereas only some residue of ethanol and acetaldehyde are detectable

247 suggesting that their degradation is still occurring. The spectrum recorded at 422°C shows only the
248 strong doublets of CO_2 and NO_2 suggesting that the degradation of all organic matter and nitrate
249 ions was completed. At 533°C NO_2 evolves as end-product of nitrate degradation, whereas the low
250 amount of CO_2 is due to the degradation process of calcium carbonate [43].
251 The thermal behaviour of Z90HAp10 is very similar to that of pure ZrO_2 (Z). In the FTIR spectra at
252 95°C and 144°C the sample release only adsorbed water and propanol. The thermal decomposition
253 of the acetylacetone leads to the formation of acetone, CO and CO_2 (in the spectrum at 198°C
254 signals were found at 1745 cm^{-1}, 1220 cm^{-1}-and 1365 cm^{-1}, respectively), whereas only a residue of
255 propanol is still visible as a weak band at 1065 cm^{-1}. Moreover, the sharp band at 948 cm^{-1} suggests
256 that also the degradation of ethanol takes place leading to the formation of ethylene. The
257 contemporary presence of the zirconia and HAp phases in this material induces a shift toward
258 higher values of the degradation temperature of acetylacetone, in comparison with that of pure
259 zirconia (115°C), and a decrease of the ethanol degradation temperature with respect to that of pure
260 HAp (263°C). Therefore, the degradation phenomena take place at the same temperature (198°C),
261 leading to a strong exothermic effect and the evolution of high amount of gas species that caused
262 the ejection of mass from the crucible during the experiment. At 554°C the degradation of all
263 organic matter was completed and only the band of CO and CO_2 are visible.
264 The first two FTIR spectra of Z70HAp30 collected at 128 and 166°C (Fig. 4), show the release of
265 adsorbed water. At 166°C also CO and CO_2 were detected, suggesting that at this temperature in
266 this sample the partial combustion of organic matter occurs as well as in pure HAp. In the spectrum
267 collected at 248 °C the degradation of the nitrate ions leads to the formation of the typical signal of
268 nitrogen oxides [46].
269 Moreover, an increase of the CO_2 release is shown, due to the degradation of organic matter. At this
270 temperature, also in this sample a weak explosion occurred, probably caused by the overlapping of
271 more exothermic degradation phenomena accompanied by the release of significant amount of gas
272 species. The gas mixture collected at 563°C contains only a residue of CO_2 and the duplet

ascribable to the formation of NO_2, suggesting that the degradation processes of organic matter and of nitrate ions are completed in this temperature conditions.

The thermal behaviour and the degradation mechanisms of Z50HAp50 is more similar to those of pure HAp with respect to those of pure ZrO_2, producing some of the gas species observed for the former, even though they were released at different temperature. The first evolution of gas was observed at lower temperature than for pure HAp (90 °C) and corresponds to water and CO_2. Therefore, the recorded spectrum is very similar to background. Also the presence of the stretching band of N=O due to the gas species produced by the degradation of nitrate ions, was found in the spectrum at 160°C, which is lower than that for pure HAp, and in that at 188°C. The spectrum at 247°C reveals the development of ethyl phosphate, produced by the reaction of ethanol with P_2O_5 [49], leading to consumption of ethanol that could explain its absence in the spectrum. Moreover, its formation delays the evolution of heat due to the alcohol degradation. Therefore, a release of a lower amount of energy occurred, thus avoiding explosive phenomena. The spectrum at 303 °C reveals the presence of ethylene, which could be due to the degradation of the ethyl phosphate [50]. Finally, NO_2 and CO_2 were detected from the spectrum at 561°C, formed at the end of nitrate degradation and decomposition of calcium carbonate. The release of CO_2 is confirmed also in the spectrum at 667°C, as final thermal degradation product of all the organic molecules and carbonate.

Fig. 5 shows the FTIR spectra of the gas mixture evolved during the TG experiments of all the samples treated at 120°C. This post-synthesis treatment leads to the removal of a part of the solvents. Therefore, apart from this low temperature process, the degradation products seem to be the same of fresh samples, thus suggesting that the thermal degradation occurring in those samples follow the same mechanisms described for the untreated samples. However, the evolution of the gaseous species for samples treated at 120°C takes place, in some cases, at temperatures slightly higher than those of fresh ones.

Therefore, the obtained results show that in all samples the complete degradation of the organic matter and nitrate ions require heating up to about 600°C. A post-synthesis heat treatment of the

gels at lower temperature, thus, could be inadequate to prepare materials potentially suitable to be used as biomaterials, because the absence of toxic by-products is an essential requirement prior of their use.

XRD structural study of the composite materials treated at 600 and 1200°C

The XRD spectra of the composite materials investigated (Z90HAp10, 70HAp30, Z50HAp50) pretreated at 120°C revealed that they are amorphous, while those of the samples calcined at 600 and 1000°C (including Z and HAp) were reported in Figs. 6 and 7, respectively.

As far as the samples treated at 600°C are concerned, Fig. 6a shows the XRD spectrum of pure HAp that does not reveal the presence of calcium phosphate, but only of a small content of calcium oxide. By increasing the amount of Z in the composites (from 50 to 90 mol%) in Fig.6b-d the degree of crystallinity decreases: Z90HAp10 is substantially amorphous, even if treated at 600°C), while Z is found to be present as a mixture of monoclinic and tetragonal phases (*t*-ZrO_2 and *m*-ZrO_2, respectively, in Fig. 6e), with an evident broadening of peaks that suggests the low degree of crystallinity for both phases.

As expected, the XRD spectra of the samples treated at 1000°C revealed in Fig. 7 an increase of the degree of crystallinity accompanied by well-defined peaks in almost all the spectra (except for plot d, related to Z90HAp10). Several crystalline phases have been identified in Fig. 7a, whose main ones are hydroxyapatite and calcium phosphate [51], along with small amount of calcium oxide [52]. Similarly to what observed for the composite materials treated at 600°C, also for those treated at 1000°C it is evident that crystallinity decreases with increasing the content of Z, being the intensities and the sharpness of peaks in plot d (related to Z90HAp10) significantly smoothed. Z treated at 1000 (Fig. 7e) is crystallized in the monoclinic system.

Two important concluding remarks can be drawn regarding the structural study. First, pure Z crystallizes at 1000°C in one phase (monoclinic one), but the presence of HAp, as a composite material, enables the crystallization in the tetragonal phase. Second, the increasing content of Z

causes an increase in the amorphization degree of all the HAp-based composites treated at 600 and 1000°.

The observed structural modifications are in agreement with the results obtained on the same materials by FTIR spectroscopy in a previous recent study [30], and affect remarkably the biological properties of the investigated materials. The material heated at 1000°C showed higher biocompatibility, explained previously in terms of an higher ability to absorb blood protein for the cell adhesion [30]. This ability is influenced by the release of ions from these materials [53], which affects the surface charge and, in turn, is affected by the crystallization degree [31].

Conclusion

The thermal behavior of pure zirconia, hydroxyapatite and of three zirconia/hydroxyapatite composite materials has been investigated under inert atmosphere by TG coupled by FTIR to analyze the gases evolved during the occurrence of each thermally stimulated process. Moreover, the structural modification of the samples caused by the thermal treatment was investigated by XRD. The results obtained in the present study allow identifying the temperatures able to induce specific degradation phenomena or structural reorganization, that are essential information to develop a materials potentially suitable to be used as biomaterials. The correlation of those data with the known biological performances showed by the same ZrO_2/HAp composites as a function of the post-synthesis heat-treatment, along with further information (e.g. identification of the ions released from the materials, of the activated biochemical pathways, of the induced cell cycle alteration, etc.) could be a useful tools to explain the mechanisms driving the biological response to these materials.

Reference

[1] O.S. Abd El-Ghany, A.H. Sherief, Zirconia based ceramics, some clinical and biological aspects: Review, Future Dental Journal, 2 (2016) 55-64.

[2] M. Catauro, F. Bollino, F. Papale, S. Pacifico, S. Galasso, C. Ferrara, P. Mustarelli, Synthesis of zirconia/polyethylene glycol hybrid materials by sol-gel processing and connections between structure and release kinetic of indomethacin, Drug Delivery, 21 (2014) 595-604.

[3] H. Harianawala, M. Kheur, S. Kheur, T. Sethi, A. Bal, M. Burhanpurwala, F. Sayed, Biocompatibility of Zirconia, Journal of Advanced Medical and Dental Sciences Research, 4 (2016) 35-39.

[4] M. Catauro, F. Papale, F. Bollino, M. Gallicchio, S. Pacifico, Biological evaluation of zirconia/PEG hybrid materials synthesized via sol-gel technique, Materials Science and Engineering C, 40 (2014) 253-259.

[5] T.R. Ramesh, M. Gangaiah, P.V. Harish, U. Krishnakumar, B. Nandakishore, Zirconia Ceramics as a Dental Biomaterial – An Over view, Trends in Biomaterials and Artificial Organs, 26 (2012) 154-160.

[6] M.R. Saeri, A. Afshar, M. Ghorbani, N. Ehsani, C.C. Sorrell, The wet precipitation process of hydroxyapatite, Materials Letters, 57 (2003) 4064-4069.

[7] W.-J. Shih, Y.-F. Chen, M.-C. Wang, M.-H. Hon, Crystal growth and morphology of the nano-sized hydroxyapatite powders synthesized from $CaHPO_4 \cdot 2H_2O$ and $CaCO_3$ by hydrolysis method, Journal of Crystal Growth, 270 (2004) 211-218.

[8] L. Micoli, G. Bagnasco, M. Turco, M. Trifuoggi, A. Russo Sorge, E. Fanelli, P. Pernice, A. Aronne, Vapour phase H_2O_2 decomposition on Mn based monolithic catalysts synthesized by innovative procedures, Applied Catalysis B: Environmental, 140-141 (2013) 516-522.

[9] C.C. Silva, A.G. Pinheiro, M.A.R. Miranda, J.C. Góes, A.S.B. Sombra, Structural properties of hydroxyapatite obtained by mechanosynthesis, Solid State Sciences, 5 (2003) 553-558.

374 [10] K. Venkateswarlu, A. Chandra Bose, N. Rameshbabu, X-ray peak broadening studies of
375 nanocrystalline hydroxyapatite by Williamson-Hall analysis, Phys. B (Amsterdam, Neth.), 405
376 (2010) 4256-4261.
377 [11] M. Catauro, F. Bollino, F. Papale, S. Pacifico, Modulation of indomethacin release from
378 ZrO_2/PCL hybrid multilayers synthesized via sol-gel dip coating, Journal of Drug Delivery Science
379 and Technology, 26 (2015) 10-16.
380 [12] M. Catauro, F. Bollino, F. Papale, Biocompatibility improvement of titanium implants by
381 coating with hybrid materials synthesized by sol-gel technique, Journal of Biomedical Materials
382 Research - Part A, 102 (2014) 4473-4479.
383 [13] M. Catauro, F. Bollino, F. Papale, Preparation, characterization, and biological properties of
384 organic-inorganic nanocomposite coatings on titanium substrates prepared by sol-gel, Journal of
385 Biomedical Materials Research - Part A, 102 (2014) 392-399.
386 [14] M. Catauro, F. Bollino, F. Papale, R. Giovanardi, P. Veronesi, Corrosion behavior and
387 mechanical properties of bioactive sol-gel coatings on titanium implants, Materials Science and
388 Engineering C, 43 (2014) 375-382.
389 [15] M. Catauro, F. Bollino, F. Papale, P. Mozetic, A. Rainer, M. Trombetta, Biological response of
390 human mesenchymal stromal cells to titanium grade 4 implants coated with PCL/ZrO_2 hybrid
391 materials synthesized by sol-gel route: In vitro evaluation, Materials Science and Engineering C, 45
392 (2014) 395-401.
393 [16] A.G. Evans, A.H. Heuer, REVIEW—Transformation Toughening in Ceramics: Martensitic
394 Transformations in Crack-Tip Stress Fields, Journal of the American Ceramic Society, 63 (1980)
395 241-248.
396 [17] P. Coli, S. Karlsson, Fit of a New Pressure-Sintered Zirconium Dioxide Coping, The
397 International journal of prosthodontics, 17 (2004) 59-64.

[18] A. Balamurugan, G. Balossier, S. Kannan, J. Michel, A.H.S. Rebelo, J.M.F. Ferreira, Development and in vitro characterization of sol-gel derived $CaO-P_2O_5-SiO_2-ZnO$ bioglass, Acta Biomaterialia, 3 (2007) 255-262.

[19] D. Bizari, M. Rabiee, F. Moztarzadeh, M. Tahriri, S.H. Alavi, R. Masaeli, Synthesis, characterization and biological evaluation of sol-gel derived nanomaterial in the ternary system 64% SiO_2 - 31% CaO - 5% P_2O_5 as a bioactive glass: in vitro study, Ceramics-Silikaty, 57 (2013) 201-209.

[20] P.I. Haris, P. Saravanapavan, J.R. Jones, S. Verrier, R. Beilby, V.J. Shirtliff, L.L. Hench, J.M. Polak, Binary $CaO-SiO_2$ gel-glasses for biomedical applications, Bio-Medical Materials and Engineering, 14 (2004) 467-486.

[21] L.L. Hench, Bioceramics, Journal of the American Ceramic Society, 81 (1998) 1705-1728.

[22] W. Habraken, P. Habibovic, M. Epple, M. Bohner, Calcium phosphates in biomedical applications: materials for the future?, Materials Today, 19 (2016) 69-87.

[23] J. Zhang, W. Liu, V. Schnitzler, F. Tancret, J.-M. Bouler, Calcium phosphate cements for bone substitution: Chemistry, handling and mechanical properties, Acta Biomaterialia, 10 (2014) 1035-1049.

[24] T. Kokubo, Bioactive glass ceramics: properties and applications, Biomaterials, 12 (1991) 155-163.

[25] L.L. Hench, Bioceramics, J. Am. Ceram. Soc., 81 (1998) 1705-1728.

[26] S. Salehi, M.H. Fathi, Fabrication and characterization of sol–gel derived hydroxyapatite/zirconia composite nanopowders with various yttria contents, Ceramics International, 36 (2010) 1659-1667.

[27] D. Qiu, A. Wang, Y. Yin, Characterization and corrosion behavior of hydroxyapatite/zirconia composite coating on NiTi fabricated by electrochemical deposition, Applied Surface Science, 257 (2010) 1774-1778.

[28] Y. Say, B. Aksakal, Effects of hydroxyapatite/Zr and bioglass/Zr coatings on morphology and corrosion behaviour of Rex-734 alloy, Journal of Materials Science: Materials in Medicine, 27 (2016) 105.

[29] D.-j. Kong, D. Long, Y.-z. Wu, C.-z. Zhou, Mechanical properties of hydroxyapatite-zirconia coatings prepared by magnetron sputtering, Transactions of Nonferrous Metals Society of China, 22 (2012) 104-110.

[30] F. Bollino, E. Armenia, E. Tranquillo, Zirconia/hydroxyapatite composites synthesized via sol-gel: Influence of hydroxyapatite content and heating on their biological properties, Materials, 10 (2017).

[31] M. Catauro, F. Bollino, R.A. Renella, F. Papale, Sol-gel synthesis of SiO_2-CaO-P_2O_5 glasses: Influence of the heat treatment on their bioactivity and biocompatibility, Ceramics International, 41 (2015) 12578-12588.

[32] M. Catauro, F. Bollino, A. Dell'Era, S. Vecchio Ciprioti, Pure $Al_2O_3 \cdot 2SiO_2$ synthesized via a sol-gel technique as a raw material to replace metakaolin: Chemical and structural characterization and thermal behavior, Ceramics International, 42 (2016) 16303-16309.

[33] M. Catauro, F. Bollino, F. Papale, S. Vecchio Ciprioti, Investigation on bioactivity, biocompatibility, thermal behavior and antibacterial properties of calcium silicate glass coatings containing Ag, Journal of Non-Crystalline Solids, 422 (2015) 16-22.

[34] M. Catauro, A. Dell'Era, S. Vecchio Ciprioti, Synthesis, structural, spectroscopic and thermoanalytical study of sol-gel derived SiO_2-CaO-P_2O_5 gel and ceramic materials, Thermochimica Acta, 625 (2016) 20-27.

[35] M. Catauro, R.A. Renella, F. Papale, S. Vecchio Ciprioti, Investigation of bioactivity, biocompatibility and thermal behavior of sol-gel silica glass containing a high PEG percentage, Materials Science and Engineering C, 61 (2016) 51-55.

447 [36] S. Vecchio Ciprioti, F. Bollino, E. Tranquillo, M. Catauro, Synthesis, thermal behavior and
448 physicochemical characterization of ZrO_2/PEG inorganic/organic hybrid materials via sol–gel
449 technique, Journal of Thermal Analysis and Calorimetry, 130 (2017) 535-540.
450 [37] S. Vecchio Ciprioti, M. Catauro, Synthesis, structural and thermal behavior study of four Ca-
451 containing silicate gel-glasses: Activation energies of their dehydration and dehydroxylation
452 processes, Journal of Thermal Analysis and Calorimetry, 123 (2016) 2091-2101.
453 [38] S. Vecchio Ciprioti, M. Catauro, F. Bollino, R. Tuffi, Thermal behavior and dehydration
454 kinetic study of SiO_2/PEG hybrid gel glasses, Polymer Engineering and Science, 57 (2017) 606-
455 612.
456 [39] S. Materazzi, S. Vecchio, L.W. Wo, S. De Angelis Curtis, TG-MS and TG-FTIR studies of
457 imidazole-substituted coordination compounds: Co(II) and Ni(II)-complexes of bis(1-
458 methylimidazol-2-yl)ketone, Thermochimica Acta, 543 (2012) 183-187.
459 [40] J. Von Hoene, R.G. Charles, W.M. Hickam, Thermal Decomposition of Metal
460 Acetylacetonates: Mass Spectrometer Studies, The Journal of Physical Chemistry, 62 (1958) 1098-
461 1101.
462 [41] I. Georgieva, N. Danchova, S. Gutzov, N. Trendafilova, DFT modeling, UV-Vis and IR
463 spectroscopic study of acetylacetone-modified zirconia sol-gel materials, Journal of Molecular
464 Modeling, 18 (2012) 2409-2422.
465 [42] M. Picquart, T. López, R. Gómez, E. Torres, A. Moreno, J. Garcia, Dehydration and
466 crystallization process in sol-gel zirconia, Journal of Thermal Analysis and Calorimetry, 76 (2004)
467 755-761.
468 [43] D.-M. Liu, Q. Yang, T. Troczynski, W.J. Tseng, Structural evolution of sol-gel-derived
469 hydroxyapatite, Biomaterials, 23 (2002) 1679-1687.
470 [44] A. Costescu, I. Pasuk, F. Ungureanu, A. Dinischiotu, M. Costache, F. Huneau, S. Galaup, P. Le
471 Coustumer, D. Predoi, Physicochemical properties of nano-sized hexagonal hydroxyapatite powder

synthesized by sol-gel method, Digest Journal of Nanomaterials and Biostructures, 5 (2010) 989-1000.

[45] W. Brockner, C. Ehrhardt, M. Gjikaj, Thermal decomposition of nickel nitrate hexahydrate, $Ni(NO_3)_2 \cdot 6H_2O$, in comparison to $Co(NO_3)_2 \cdot 6H_2O$ and $Ca(NO_3)_2 \cdot 4H_2O$, Thermochim. Acta, 456 (2007) 64-68.

[46] P. Melnikov, V.A. Nascimento, I.V. Arkhangelsky, L.Z. Zanoni Consolo, Thermal decomposition mechanism of aluminum nitrate octahydrate and characterization of intermediate products by the technique of computerized modeling, Journal of Thermal Analysis and Calorimetry, 111 (2013) 543-548.

[47] H.E. Morris, Reactions of Ethyl Alcohol, Chemical Reviews, 10 (1932) 465-506.

[48] J. Coates, Interpretation of Infrared Spectra, A Practical Approach, in: R. Meyers (Ed.) Encyclopedia of Analytical Chemistry, John Wiley & Sons Ltd, Chichester, 2000, pp. 10815–10837.

[49] M. Zangen, E.D. Bergmann, Y. Marcus, Products of the Reaction Between Alcohols and Phosphorus Pentoxide. III. Identification by Infrared Spectrophotometry, Israel Journal of Chemistry, 5 (1967) 89-100.

[50] E.J.P. Zegers, E. Fisher, Pyrolysis of Triethyl Phosphate, 1998.

[51] D.N. Ungureanu, N. Angelescu, R.M. Ion, E.V. Stoian, C.Z. Rizescu, Synthesis and Characterization of Hydroxyapatite Nanopowders by Chemical Precipitation, Recent Researches in Communications, Automation, Signal Processing, Nanotechnology, Astronomy and Nuclear Physics, WSEAS Press, Cambridge, UK, 2011.

[52] N.H.A. Camargo, S.A. de Lima, E. Gemelli, Synthesis and Characterization of Hydroxyapatite/TiO_2 Nanocomposites for Bone Tissue Regeneration, American Journal of Biomedical Engineering, 2 (2012) 41-47.

496 [53] E. Mavropoulos, A.M. Costa, L.T. Costa, C.A. Achete, A. Mello, J.M. Granjeiro, A.M. Rossi,
497 Adsorption and bioactivity studies of albumin onto hydroxyapatite surface, Colloids and Surfaces
498 B: Biointerfaces, 83 (2011) 1-9.

Captions of the figures

Fig. 1. TG/DTG curves at 10 K min^{-1} under a nitrogen purging gas atmosphere of fresh (not thermally treated) materials.

Fig. 2. Sample temperature vs. time plots of TG experiments for: Z90HAp10 (a-c); Z70HAp30 (d-f).

Fig. 3. TG/DTG curves at 10 K min^{-1} under a nitrogen purging gas atmosphere of materials treated at 120°C.

Fig. 4. FTIR spectra of the gas mixture evolved during TG analysis at different temperatures for fresh (not thermally treated) materials.

Fig. 5. FTIR spectra of the gas mixture evolved during TG analysis at different temperatures for materials treated at 120°C.

Fig. 6. X-ray diffraction pattern of materials treated at 600°C: Z (a), Z90HAp10 (b); Z70HAp30 (c); Z50HAp50 (d); HAp (e). Phases identified: hydroxyapatite (★), *t*-ZrO_2 (#), *m*-ZrO_2 (°), calcium phosphate (+) and calcium oxide (^).

Fig. 7. X-ray diffraction pattern of materials treated at 1000°C: Z (a), Z90HAp10 (b); Z70HAp30 (c); Z50HAp50 (d); HAp (e). Phases identified: hydroxyapatite (★), *t*-ZrO_2 (#), *m*-ZrO_2 (°), calcium phosphate (+) and calcium oxide (^).

523 Fig. 1

524

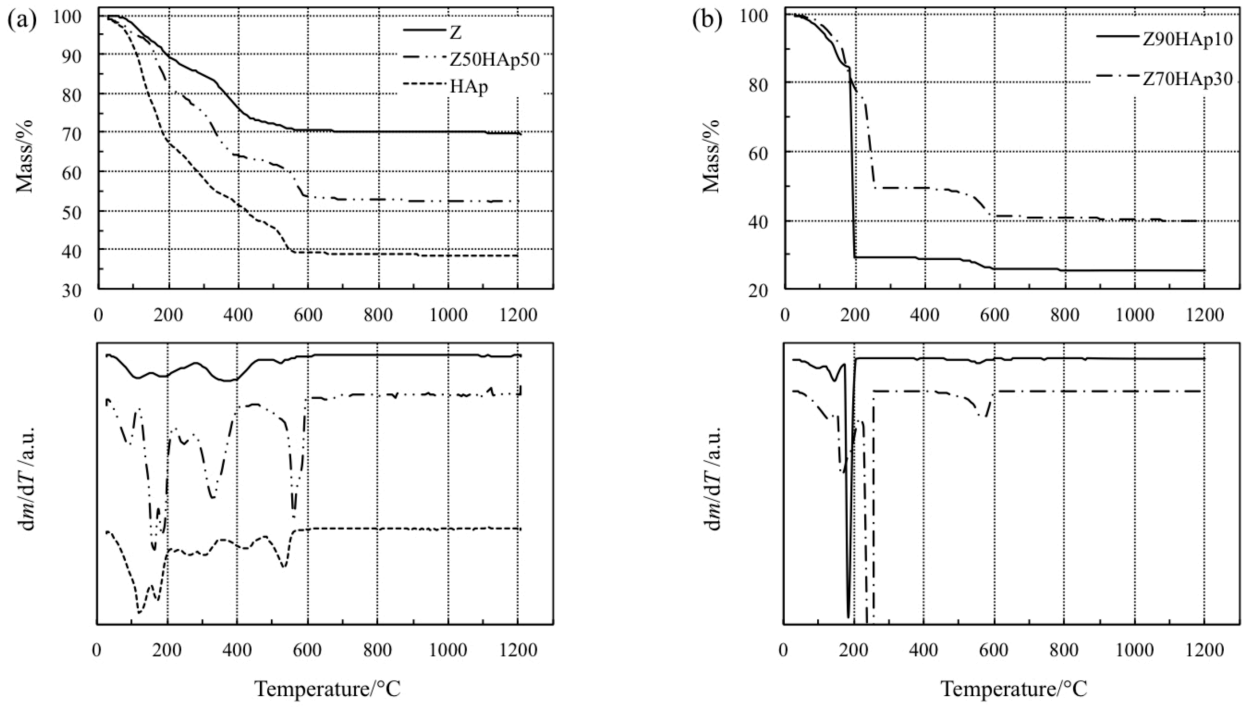

525

526

527

528 Fig. 2

529

530

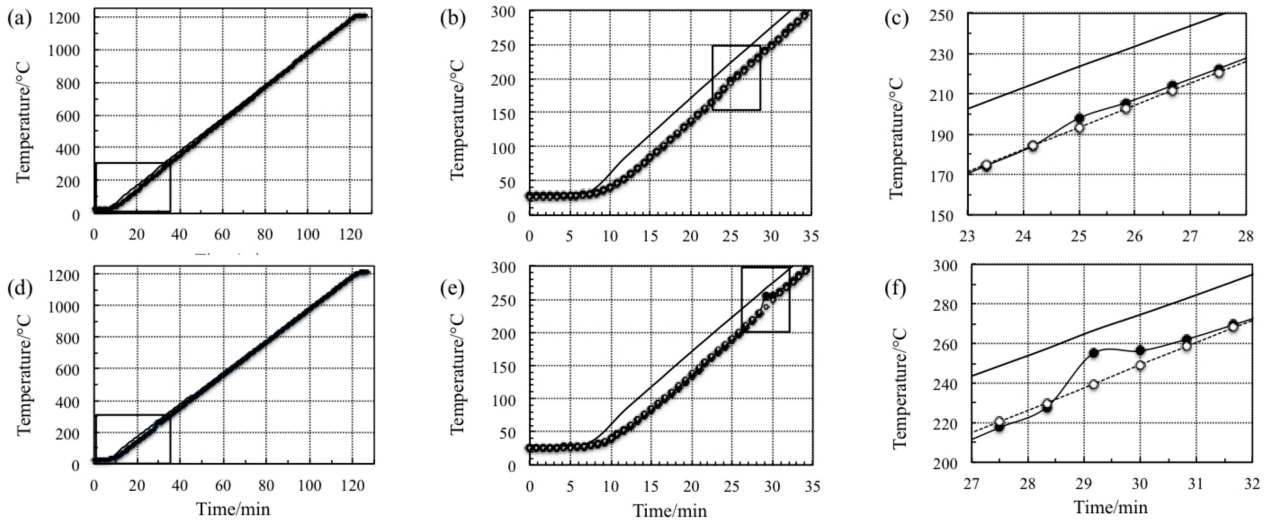

531

532

533

534 Fig. 3

535

536

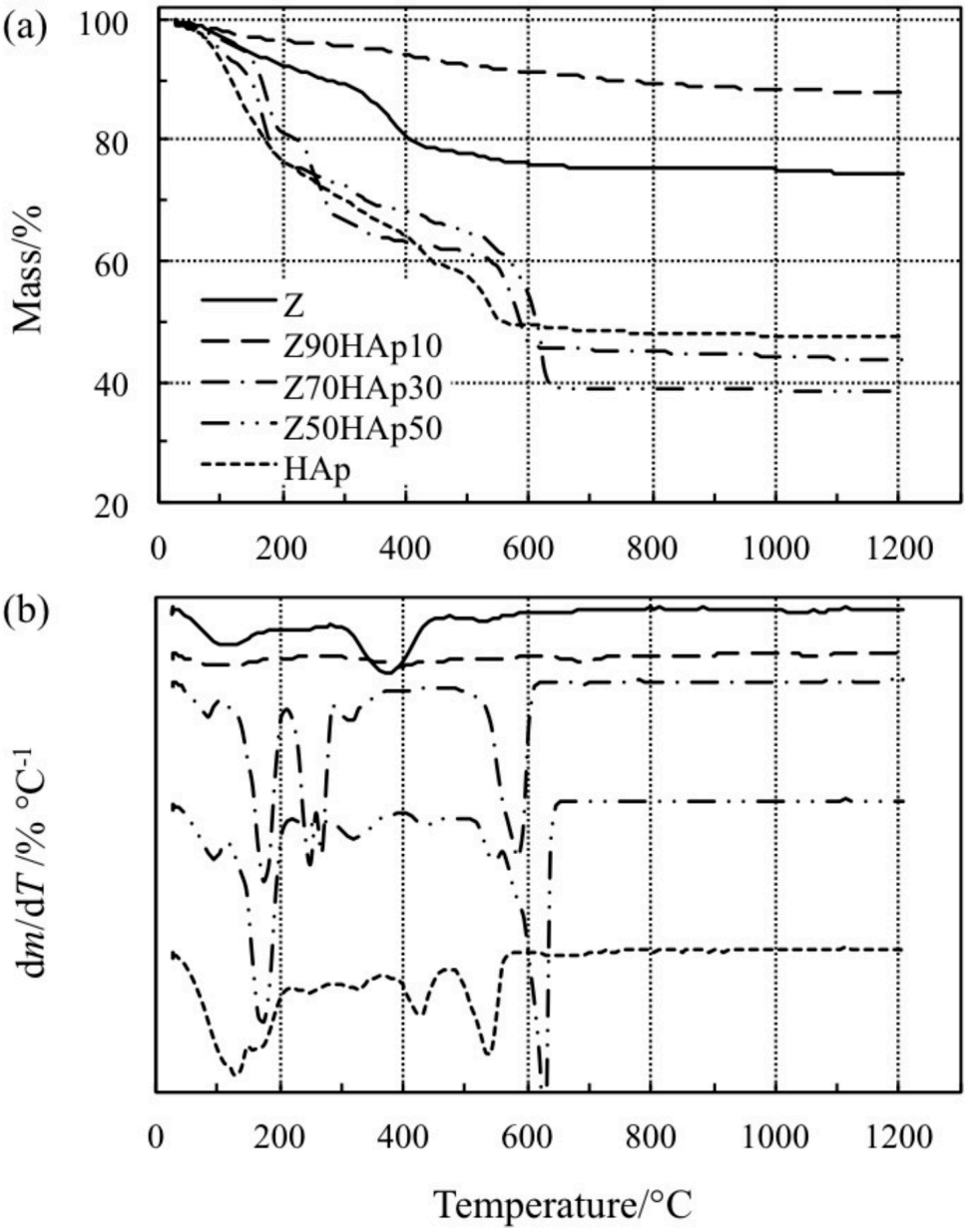

537

538

539

Fig. 4

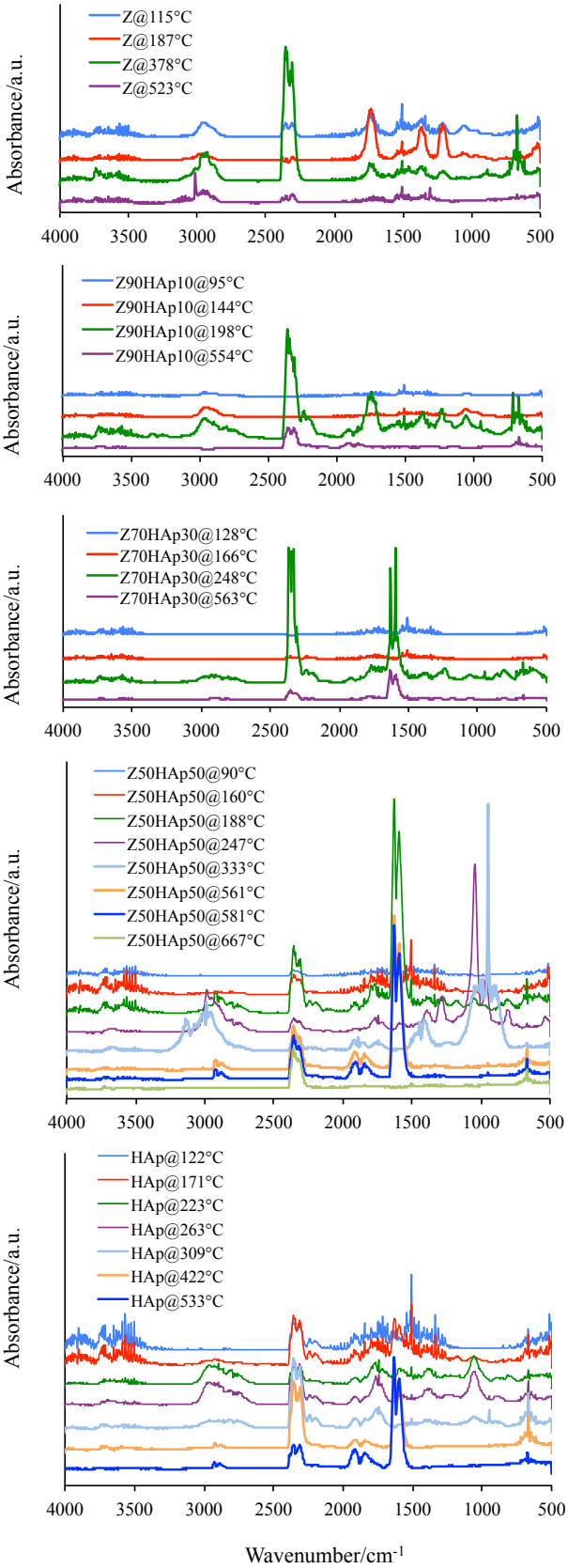
Z@115°C
Z@187°C
Z@378°C
Z@523°C
Absorbance/a.u.
Z90HAp10@95°C
Z90HAp10@144°C
Z90HAp10@198°C
Z90HAp10@554°C
Absorbance/a.u.
Z70HAp30@128°C
Z70HAp30@166°C
Z70HAp30@248°C
Z70HAp30@563°C
Absorbance/a.u.
Z50HAp50@90°C
Z50HAp50@160°C
Z50HAp50@188°C
Z50HAp50@247°C
Z50HAp50@333°C
Z50HAp50@561°C
Z50HAp50@581°C
Z50HAp50@667°C
Absorbance/a.u.
HAp@122°C
HAp@171°C
HAp@223°C
HAp@263°C
HAp@309°C
HAp@422°C
HAp@533°C
Absorbance/a.u.
4000 3500 3000 2500 2000 1500 1000 500
Wavenumber/cm-1

544 Fig. 5

545

546

547

548

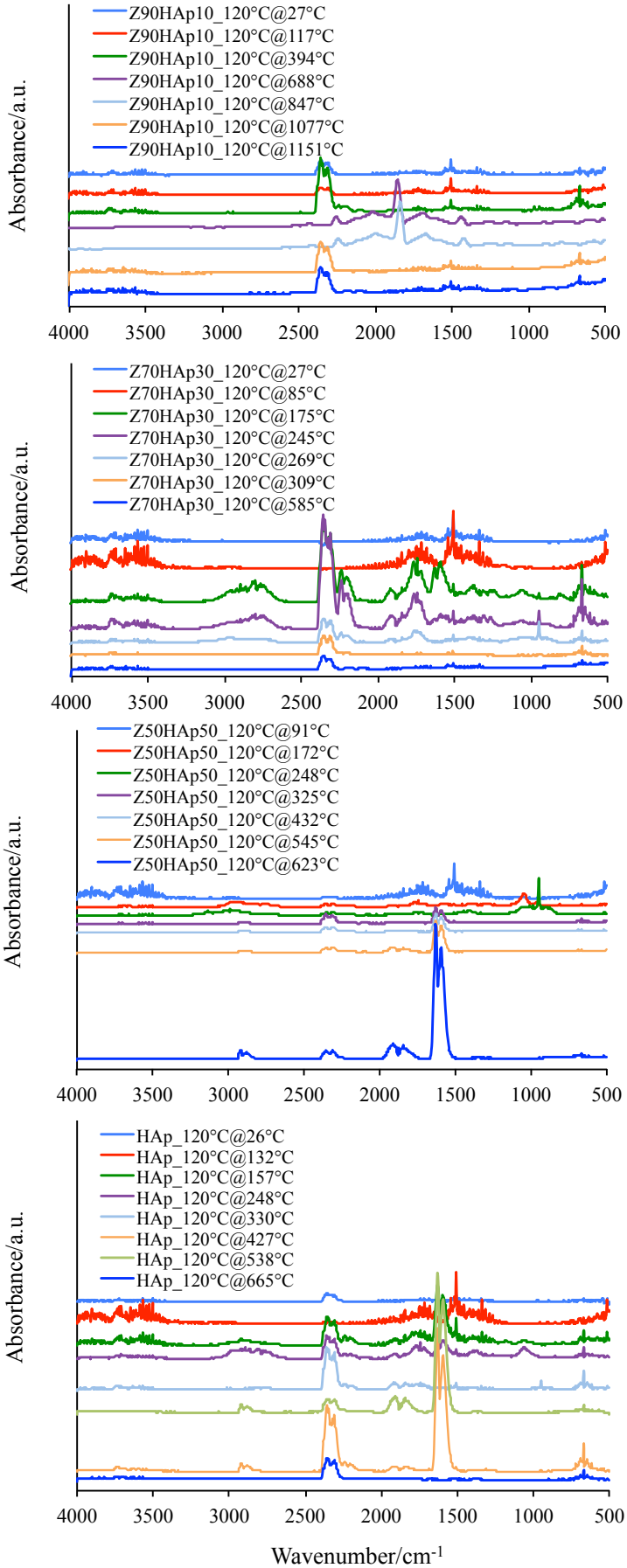

549 Fig. 6

550

551

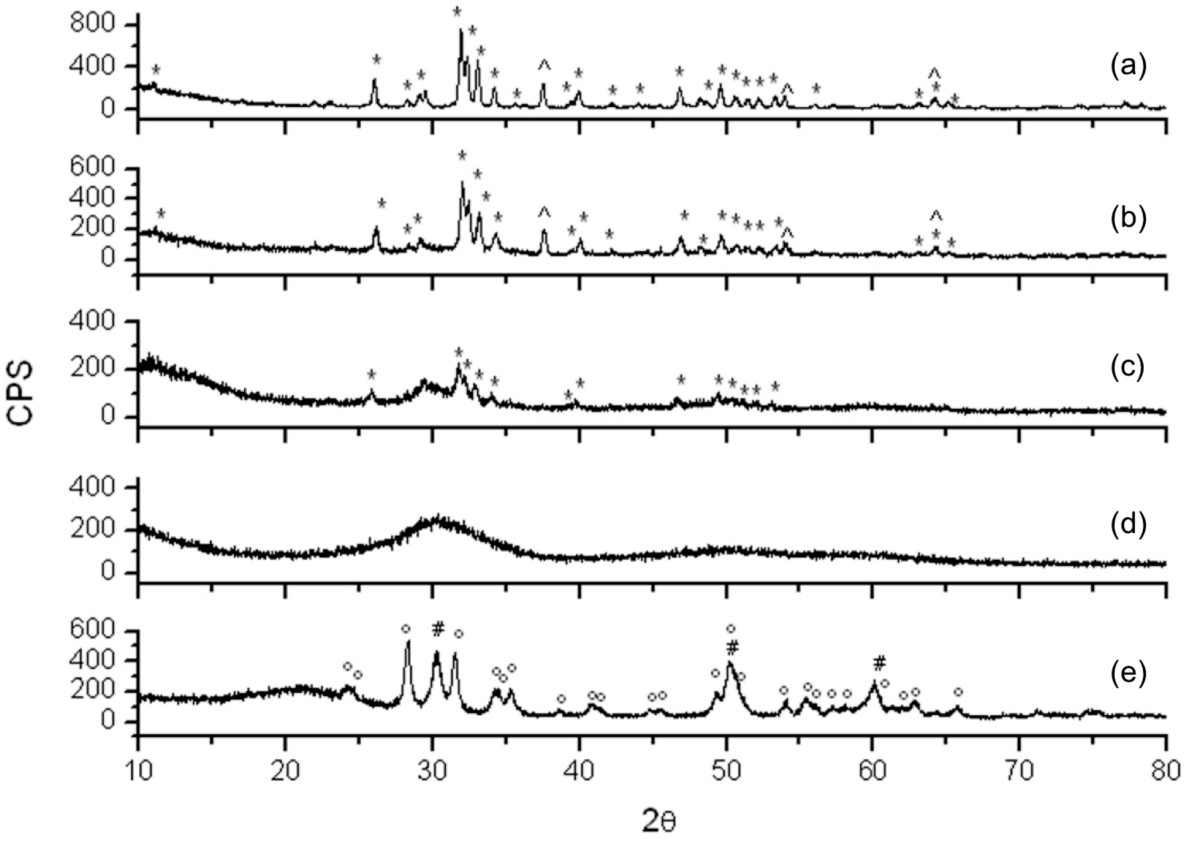

552

553

554

555 Fig. 7

556

557

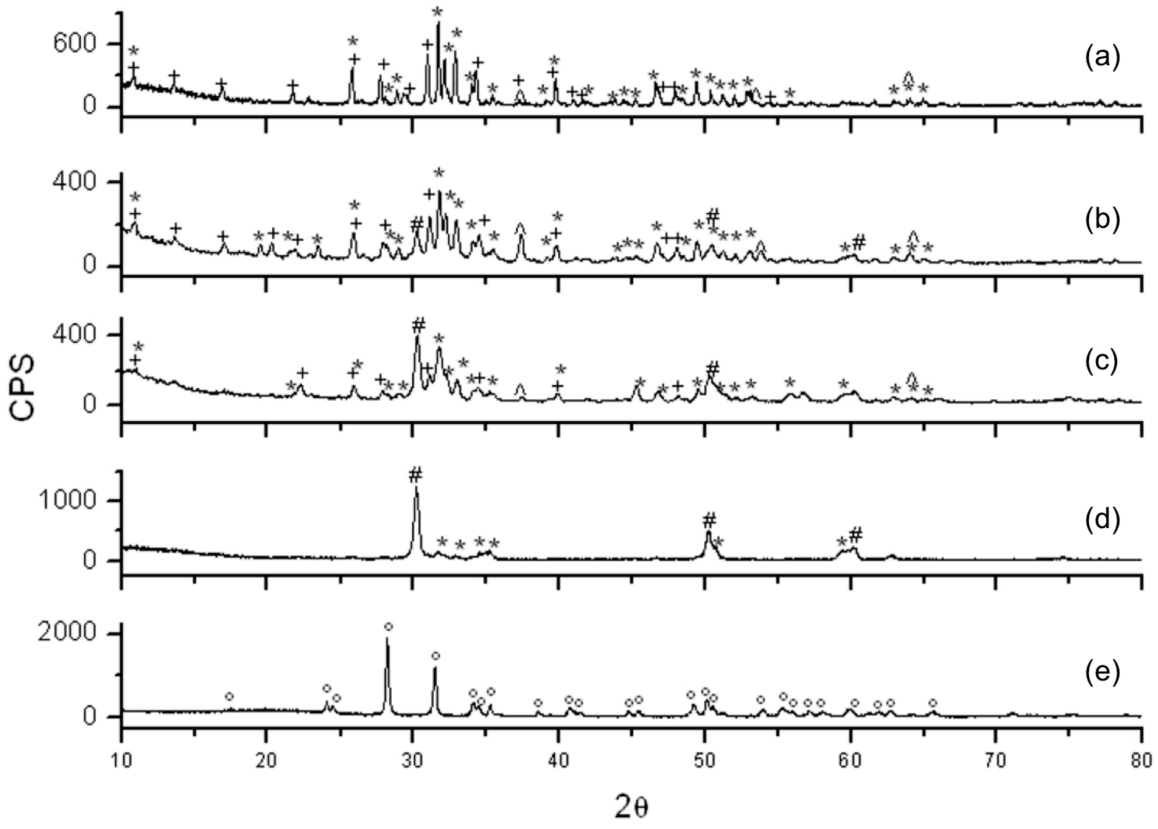

558